Solar Energy 135 (2016) 731–741

Contents lists available at ScienceDirect

Solar Energy

journal homepage: www.elsevier.com/locate/solener

A comprehensive study on partial shading response of c-Si modules and yield modeling of string inverter and module level power electronics

K. Sinapis [a,*], C. Tzikas [a,c], G. Litjens [a,b], M. van den Donker [a], W. Folkerts [a], W.G.J.H.M. van Sark [b], A. Smets [c]

[a] Solar Energy Application Centre, Eindhoven, The Netherlands
[b] Utrecht University, Copernicus Institute, Utrecht, The Netherlands
[c] Delft University, PVMD, Delft, The Netherlands

ARTICLE INFO

Article history:
Received 8 January 2016
Received in revised form 27 May 2016
Accepted 20 June 2016

Keywords:
MLPE
BIPV
Micro-inverters
Power-optimizers

ABSTRACT

Building Integrated and Building Attached Photovoltaic (BIPV, BAPV) systems may suffer from lower performance than predicted as a result of not considered partial shading. New system architectures have been proposed to optimize performance. The common approach of these new architectures is to track the Maximum Power Point (MPP) of every solar module individually. A simulation model is developed to quantify the benefits and drawbacks of different PV system architectures. The model includes a shading evaluation of the installation with means of 3D modeling, irradiance calculations, PV cell modeling and finally an empirical power conversion model. The energy yield of three leading architectures is confirmed (string inverter, power optimizer, micro inverter) for clear and partial shading conditions by means of an outdoor field test. Results with the irradiance profile of the Netherlands show that the string inverter system outperforms MLPE in 2 out of 3 partial shading scenarios that were evaluated in this study. It is found that the energy yield benefit of MLPE has a seasonal and latitude variation with the highest contribution during winter months. Additionally a study was performed to evaluate the energy yield at different irradiance profiles. Results show that there is a marginal benefit of the micro inverter system at higher irradiance locations when partial shading is present. The analysis method can be used by PV installers and system designer to determine which is the optimal system architecture for maximum energy yield especially when partial shading is present.

1. Introduction

Penetration of solar photovoltaic (PV) systems in the Netherlands and worldwide has remarkably increased the past years and it is forecasted to keep growing in the future (IEA PVPS Annual Report, 2014). Particularly the application of BIPV and BAPV systems are projected to thrive in the following years as a result of increasing electricity prices for the residential sector and decreasing PV component costs. Residential and small commercial PV systems are typically installed in an urban environment. Roofs and terraces are often affected by shade coming from the close proximity of buildings, poles, antennas, dormers, etc. and thus introduce electrical and thermal mismatch losses between cells and modules. These are generally caused by manufacturing tolerance, heterogeneous irradiation conditions which are especially important for larger systems, module degradation and thermal mismatch of the solar modules. Solar modules are connected in series and thus sharing the same current in a string. This topology is prone to power losses if the solar cells in the module are not operating under the same conditions thereby reducing the current of the module and consequently of the whole string. Partially shaded solar cells may become reverse biased because of the series connection and thus act as a load consuming the power that is generated by the unshaded cells. Two negative effects occur from partially shaded operation of a PV system: power loss and increased temperature of the shaded cells (hot-spot). By-pass diodes have been applied in solar modules to prevent power consumption from shaded cells and to prevent hot-spots by by-passing the shaded substrings of the solar module. Most of the solar modules include one by-pass diode connected anti parallel per 16–24 cells (Silvestre et al., 2009).

The use of module level power electronic devices (MLPE) has been proposed to mitigate electrical and thermal mismatch losses (Poshtkouhi et al., 2012; Woyte et al., 2003; Hanson et al., 2014) in the field by tracking the maximum power point of individual modules. In general MLPE devices consist of two main categories: micro inverters and power optimizers. In this paper micro inverters and

* Corresponding author.
E-mail addresses: kostas.sin@hotmail.com, sinapis@ecn.nl (K. Sinapis).

http://dx.doi.org/10.1016/j.solener.2016.06.050
0038-092X/

boost power optimizers are considered. The boost power optimizers are installed behind the solar modules and connected in parallel through a trunk cable, creating a 380 V DC voltage. Subsequently a central inverter is utilized to convert the DC power to AC.

Although modeling tools have been developed based on a variety of software platforms, most of them don't consider the system architecture. There are many available models which can be different in terms of mathematical sub-models and assumptions. Some models lack transparency and as a result project developers are expressing concerns regarding PV performance validity forecast, especially when shading is present. The key challenges of partial shading PV models is therefore to generate accurate yield predictions under heterogeneous irradiance conditions with reduced simulation time. In this paper a model is presented that considers cell shading fractions determined by a 3D model and applies an irradiance model to determine the effective irradiance on a partially shaded cell. Moreover, the model takes into consideration the system architecture and associated power electronics efficiency losses.

2. Correlations of shading fraction and power output at c-Si solar modules

A steady state solar simulator (Batzelis et al., 2015) was utilized for a series of shading experiments on a solar module with 60 series connected monocrystalline silicon cells. The module consists of 3 groups of 20 cells and each group is connected anti-parallel with a by-pass diode. An IV tracer was recording performance under standard test conditions (25 °C, 1000 W/m^2 irradiance). Artificial shading was applied with two means: (a) opaque masking with black cardboard and (b) wire meshes with reduced transmittance as seen in Fig. 2.1. The reason of using two shading strategies is to represent field conditions where the beam B irradiance is obstructed and sky diffuse D remains relatively the same. In Fig. 2.2 the spectral transmittance of the wire meshes is shown. For the analysis the 33% and 67% transmittance were chosen to fit realistic D/G ratio.

Measurements were performed for cell shading percentages of: 10%, 15%, 20%, 25%, 30%, 35%, 40%, 50%, 75% and 100% with three transmittance levels 0%, 33% and 67%. Twelve different cells were shaded for every shading fraction giving a total of 120 *I–V* curves per shading material in order to provide a distribution of the shade effect since the shading response is highly associated with shunt resistance of individual cells (Grunow et al., 2004). In Fig. 2.4 the relative power output in correlation with the shading fraction can be seen. As expected the opaque shading is causing the largest drop in power output. It is important to mention that even shading a very small portion of a single solar cell (10–50%) leads to disproportional losses in power output. When opaque shading as a fraction of a single solar cell's surface exceeds 50% then there is a total reduction of power at that cell's group due to the activation of the by-pass diode. Thus further shading of the specific cell or group of cells will not have any consequence in power output. These results are supported by similar work in the field (Deline, 2009). For the meshed cell shading more coverage is needed to acquire the same results as in opaque shading fraction.

From Fig. 2.3 one can determine the relative effective shading fraction by comparing the power output for the different transmittance materials. For example the power output of the 67% transmittance mesh shading 100% of the solar cell is equivalent to 33% opaque shading. This transition can be better seen in Fig. 2.4. The results for all the three different transmittance materials fit perfectly leading to Eq. (1) which describes the effective equivalent irradiance of a partially shaded solar cell.

$$G_{cell,eff} = (\text{unshaded fraction } \% * G_k) + (\text{shaded fraction } \% * G_{diff,k}) \quad (1)$$

where

- $G_{cell,eff}$ is the effective cell irradiance
- G_k the global in-plane irradiance
- $G_{diff,k}$ the diffuse in-plane irradiance.

An application of Eq. (1) on a partially shaded solar cell can be seen in Fig. 2.5. Assuming partial shading in half the cell's surface the equivalent homogenous irradiance can be determined when the G_k and G_{diff} are known.

3. Yield model

The complete MLPM yield model includes 5 different models integrated into one. Namely, it includes a 3D SketchUp model, a shading model, a radiation model, a DC and an AC simulation model. All the model inputs used in the complete model and the flow of simulation processes are shown in Fig. 3.1. In the following sections, each one of the models will be separately presented along with all its specifics.

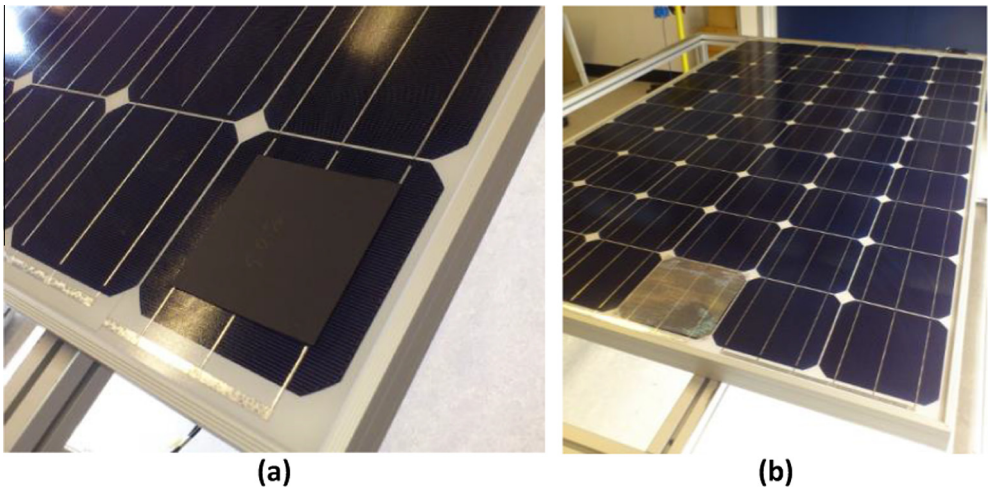

Fig. 2.1. Impression of the opaque (a) and wire meshes (b) used for the shading correlation experiments under a steady state solar simulator.

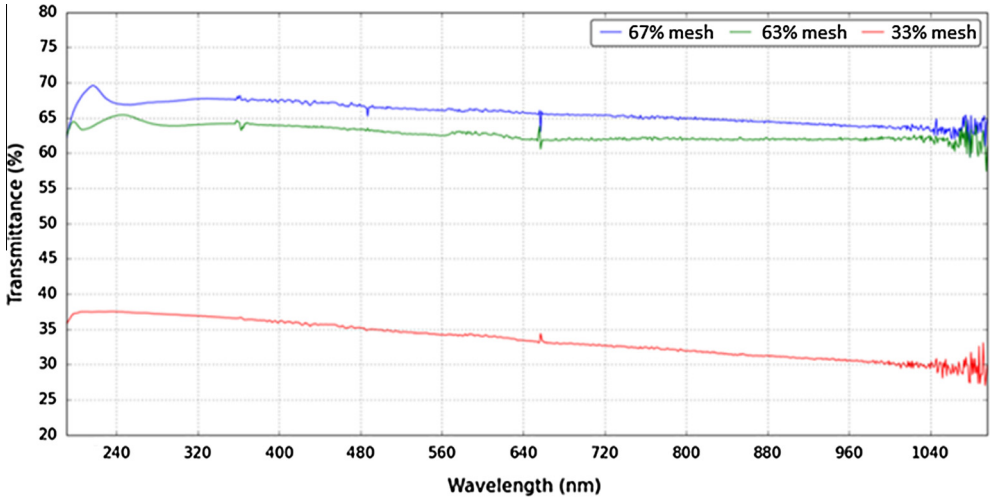

Fig. 2.2. Transmittance of the three meshes for a wide range of wavelengths.

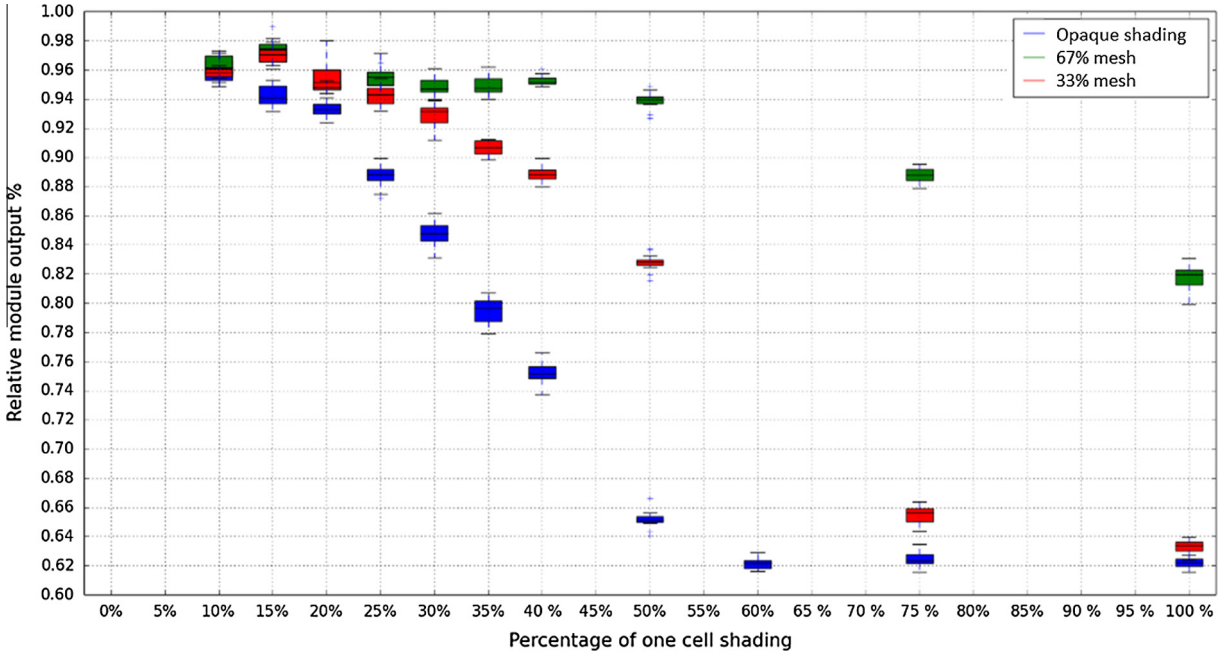

Fig. 2.3. Relative power output for various shading percentages of a cell by using wire meshes and opaque cardboard.

3.1. 3D shading model and determination of shading fraction

To accurately predict the power output and behavior of a partially shaded solar module, the shade coverage of the module's surface has to be known. For this reason, a computer-aided design tool is used to represent the installation site including the PV modules and the obstruction elements which cause the partial shading. There is a big variety of CAD software available in the market but for this study Google SketchUp (http://www.sketchup.com, 2015) is used.

Simulation procedure:

- Design an accurate representation of the installation including the PV modules and all the obstruction elements (Fig. 3.1.1).
- In SketchUp the option is provided of exporting model elements x, y, z coordinates using the point cloud extraction function. This is done by selecting the cells and obstruction elements.
- A Python script is developed to virtually re-create the shading surfaces by using the x, y, z coordinates of the cells and the obstruction elements. Given the azimuth and altitude of the sun which is modeled depending on the location (Angus and Muneer, 1993) at any particular time, simple trigonometric relationships can determine the relative X and Y offset coordinates of shadow points on a flat or inclined plane. Constructing the shadow of a complex 3D object is simply a process of translating each of its vertexes in turn to produce an outline on the ground or at a plane. The output of the model is a look up table with the shading fraction of the cells for any given azimuth and elevation angle of the sun. As a result, these look up tables can be used for various locations.

The shading fraction of each cell in the system is calculated with 0.5 degrees interval of the sun's azimuth and elevation angle. For higher accuracy the look up tables can be constructed with a range

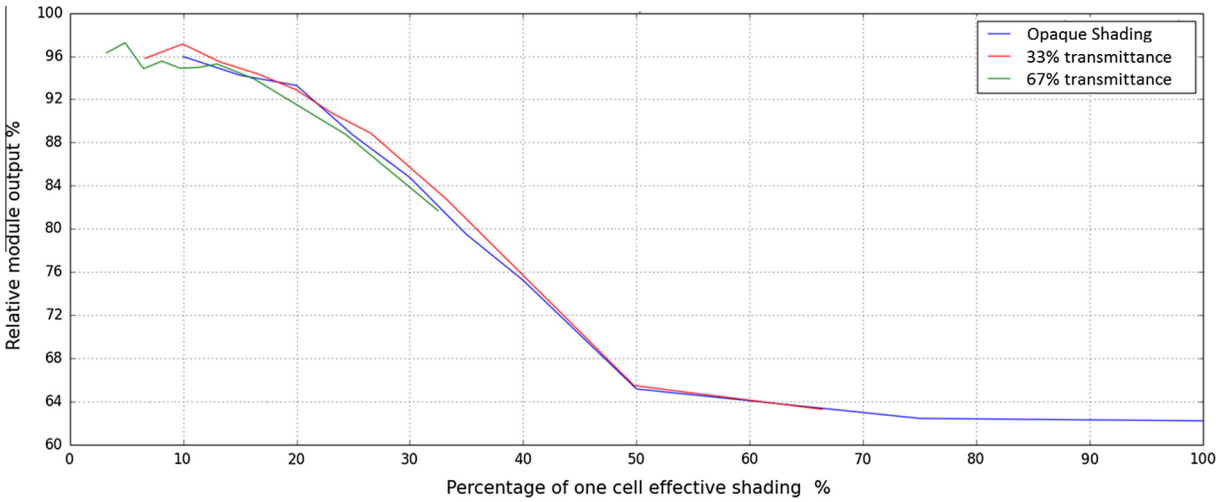

Fig. 2.4. Relative effective shading fraction versus power output for three different shading materials.

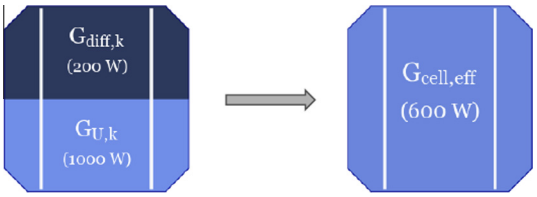

Fig. 2.5. Application of Eq. (1) for partial shading.

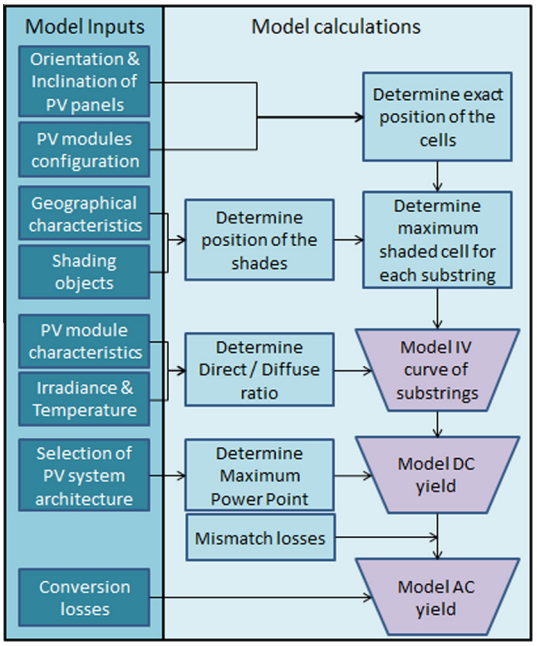

Fig. 3.1. Yield model inputs and flow of simulation processes.

of azimuth and elevation intervals with an unavoidable consequence in simulation time. In Fig. 3.1.2 a graphic representation of a part of the look up table can be seen. Specifically the shadow extension of a pole situated at the south part of the system for three different times of the day is visible. Subsequently the heaviest shaded solar cell of a substring is determined and is used as an input for the next part of the simulation.

3.2. Irradiance model for determination of direct and diffuse light components

After the determination of the shaded fraction of the cell, the diffuse and direct part of the irradiance has to be calculated with an irradiance decomposition model. A comparative review of the various irradiance models and their empirical validation has been presented by Loutzenhiser et al. (2007).

For this paper the Reindl-2 model (Reindl et al., 1990) was chosen to estimate the diffuse part of irradiance using as input the clearness index, the global horizontal irradiance and the elevation angle of the sun.

For $0 \leqslant k_t \leqslant 0.3$ and $G_{diff}/G \leqslant 1.0$:

$$\frac{G_{diff}}{G} = 1.02 - 0.254k_t + 0.0123\sin(a) \tag{2}$$

For $0.3 < k_t < 0.78$ and $0.1 \leqslant G_{diff}/G \leqslant 0.97$:

$$\frac{G_{diff}}{G} = 1.4 - 1.749k_t + 0.177\sin(a) \tag{3}$$

For $k_t \geqslant 0.78$ and $G_{diff}/G \geqslant 0.1$:

$$\frac{G_{diff}}{G} = 0.486k_t - 0.182\sin(a) \tag{4}$$

where

- G, G_{diff} are the global horizontal irradiance and the diffuse part of the irradiance respectively
- k_t is the clearness index
- a is the elevation angle of the sun.

3.3. PV cell model

A mono-crystalline cell can be modeled with the equivalent electric circuit of a simplified double diode model developed by Ishaque et al. (2011) and shown in Fig. 3.1.3.

The output current of the cell is given by Eqs. (5)–(9) (Chih-Tang et al., 1957):

$$I = I_{ph} - I_{D1} - I_{D2} - \left(\frac{V + IR_s}{R_{sh}}\right) \tag{5}$$

$$I_{D1} = I_{o1}\left[\exp\left(\frac{V + IR_s}{n_1 V_{th}}\right) - 1\right] \tag{6}$$

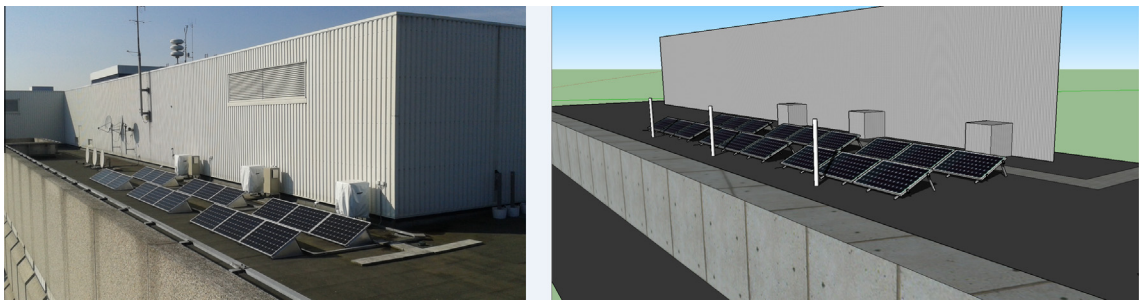

Fig. 3.1.1. Impression of the field test (left) and impression of the 3D model (right).

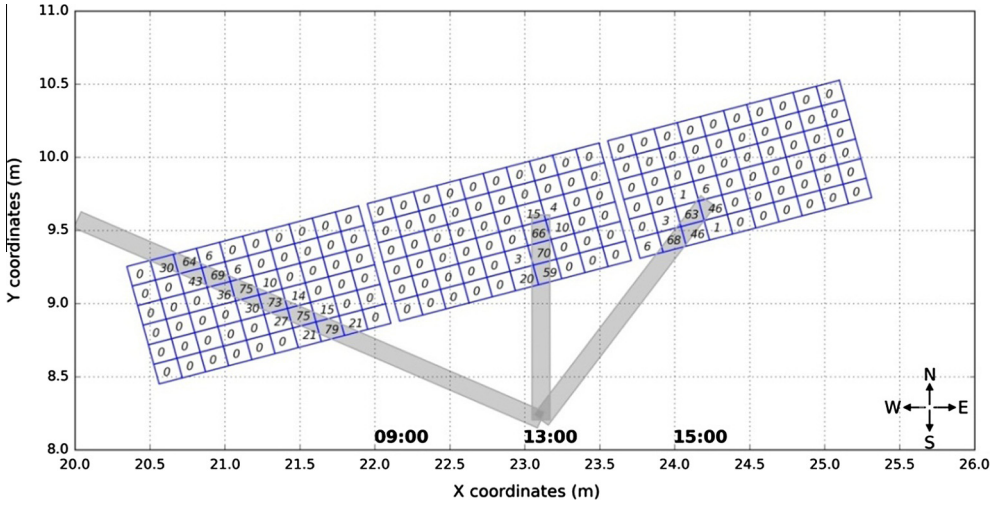

Fig. 3.1.2. Graphic representation of the look up table for specific time and date produced by the shading model.

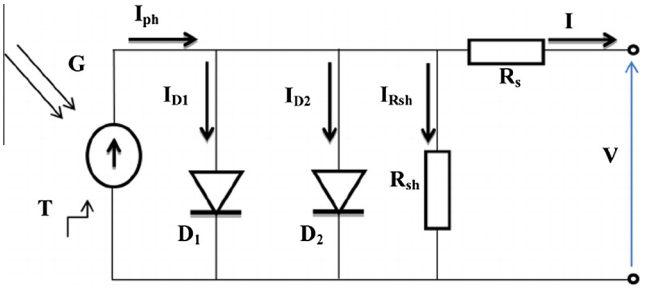

Fig. 3.1.3. Double diode equivalent circuit for a PV cell.

$$I_{D2} = I_{o2}\left[\exp\left(\frac{V + IR_s}{n_2 V_{th}}\right) - 1\right] \tag{7}$$

$$V_{th} = N_s \frac{kT}{q} \tag{8}$$

$$I_{ph} = \frac{G}{G_{STC}} I_{ph_{STC}}(1 + K_I \Delta T) \tag{9}$$

where

- I_{o1}, I_{o2} are the reverse saturation currents of the diodes D_1 and D_2 respectively
- V_{th} is the thermal voltage of the diodes
- n_1, n_2 are their quality factors of the diodes
- R_s, R_{sh} are the series and shunt resistances respectively
- k is the Boltzmann constant
- q is the electron charge
- N_s is the number of cells connected in series
- T is the module temperature
- G is the irradiance
- G_{STC} the irradiance under Standard Test Conditions (1000 W/m^2)
- $\Delta T = T_c - T_{ref}$ the temperature difference between the solar cell's temperature and the reference temperature (25 °C).

In many papers, researchers are trying to calculate separately the saturation currents of the two diodes in the double-diode cell model, but this procedure is time consuming as it greatly increases the computational time by using an iteration approach (Jinhui et al., 2009). For simplicity reasons, we assume that $I_{o1} = I_{o2} = I_o$ as shown in Ishaque et al. (2011) where the saturation current can be calculated using the equation below. This assumption eliminates the ambiguity of selecting the values n_1 and n_2 as well.

Thus the saturation current can be calculated by Eq. (10) (Carrero et al., 2010):

$$I_o = \frac{\frac{I_{sc}(R_s + R_{sh}) - V_{oc}}{R_{sh}}}{\exp\left(\frac{V_{oc}}{n_1 V_{th}}\right) + \exp\left(\frac{V_{oc}}{n_2 V_{th}}\right)} \tag{10}$$

The saturation current increases with temperature as shown by Eq. (11) (Ishaque et al., 2011):

$$I_o = I_{o_{STC}}\left(\frac{T}{T_{ref}}\right)^3 \exp\left(\frac{q}{N_1 k}\left(\frac{E_g}{T_{ref}} - \frac{E_g(T)}{T}\right)\right) \tag{11}$$

where

- E_g is the energy band gap of the semiconductor (1.12 eV for silicon)
- T_{ref} = 25 °C and $I_{o_{STC}}$ is the nominal saturation current at STC.

The simulated *I–V* and *P–V* curves with different irradiance inputs for the whole module are shown in Fig. 3.1.4. In Fig. 3.1.5 the *I–V* and *P–V* curves for inhomogeneous irradiance levels between the cell substrings are shown.

By using Eq. (1) to calculate irradiance input for the solar cell model, a look up table with *I–V* curves per substring has been created for all possible irradiance and module temperature combinations (1–1500 W/m^2 and from 0 to 100 °C with 1 W/m^2 and 1 °C intervals). This way instead of running the script for the PV module which contains complex equations and iterations, the ready-made *I–V* curves corresponding to the given conditions are called from the look up table in order to build-up the PV module's *I–V* curve, using the 3 relative *I–V* curves of the 3 substrings.

3.4. MPPT and power conversion model (DC/AC)

Nearly all modern inverters have more than 99% MPPT efficiency. While Perturb and Observe (P&O) is the most used algorithm new hybrid algorithms have been implemented by inverter manufacturers to boost performance at partial shading conditions (http://files.sma.de/dl/3491/TECHOPTITRAC-AEN082412.pdf, 2015; http://www.mastervoltsolar.com/high-yield, 2015). This is achieved by frequent scans of the *P–V* curve of the solar modules which ensure that the inverter will detect the MPP even in the case of lumpy *P–V* curves. In this study the MLPE devices are using the hybrid P&0 algorithm while the string inverter system has the option to activate it. Note that the string inverter is delivered from the manufacturer with the shadow mode deactivated. The model assumes that the MPP of the solar modules is always found and kept when the hybrid algorithm is used, however the string inverter is modeled with the hypothesis that when the shadow mode is deactivated the solar modules are operated at a local maximum when partial shading is present.

In order to develop the conversion model, real measured data where used (Sinapis et al., 2015). In Fig. 3.1.6 the relation of the conversion losses with the current and voltage input can be seen for the string inverter system. By using second degree polynomial fit the loss curves can be calculated based on different voltage and current levels.

The equations of these polynomial fits that were used in the model, along with their conditions are presented in Eqs. (12)–(17):

$$\text{For } 100 \leqslant V \leqslant 145: \quad y = 0.3772x^2 + 4.295x + 4.263 \tag{12}$$

$$\text{For } 145 < V \leqslant 155: \quad y = 0.3668x^2 + 5.096x + 3.068 \tag{13}$$

$$\text{For } 155 < V \leqslant 165: \quad y = 0.4488x^2 + 5.173x + 3.302 \tag{14}$$

$$\text{For } 165 < V \leqslant 175: \quad y = 0.4325x^2 + 5.802x + 3.013 \tag{15}$$

$$\text{For } 175 < V \leqslant 190: \quad y = 0.4419x^2 + 6.189x + 2.945 \tag{16}$$

$$\text{For } 190 < V \leqslant 230: \quad y = 0.304x^2 + 7.843x + 1.618 \tag{17}$$

Similar for the power optimizer and micro inverter system polynomial equations based on different voltage inputs have been calculated and used for the simulations. In Fig. 3.1.7 the polynomial equations are used to predict the AC yield. The DC measured data from the field test were used as an input to solve the polynomial equations for the micro inverter system. Deviation from measured and simulation were about 0.1% for the unshaded micro inverter while 1% is observed for the shaded micro inverter.

4. Model validation by using real measured data

For the validation of the proposed yield model, measurements from 3 systems in Eindhoven (Sinapis et al., 2015) are used. The systems are oriented south-east with an inclination angle of 30°. The systems architecture consists of a string inverter system, a power optimizer system and a micro inverter system, all with the same installed power (1.6 kWp). The electrical parameters are continuously monitored before and after every stage of power conversion including in plane global irradiance and module temperatures. For the model validation the measured irradiance from the field test has been used as input after having been decomposed in diffuse and direct components (Gueymard, 2009). Moreover, module temperatures have been used by the measured data.

For obstruction shading, three shading scenarios that usually occur in pitched and flat roofs have been defined:

- *Pole shading:* a pole with 1.70 m height has been positioned on the south side of the systems.
- *Row to row shading:* A wall situated on the south side of the systems (Fig. 3.1.1), homogenously shades all three systems during winter months. Additionally because of the module spacing there is row to row shading.
- *Soiling:* In central and north European climate, rain is abundant. It is a fact that framed solar modules could build up algae at the bottom part and thus obstruct completely irradiance. The more

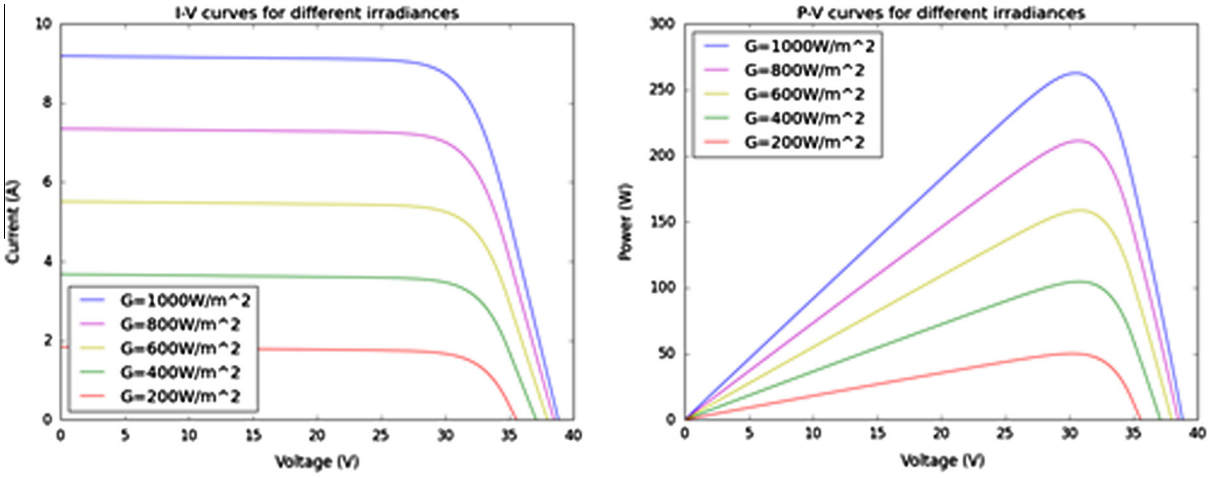

Fig. 3.1.4. Simulated *I–V* and *P–V* curves for the solar module for homogeneous irradiance levels.

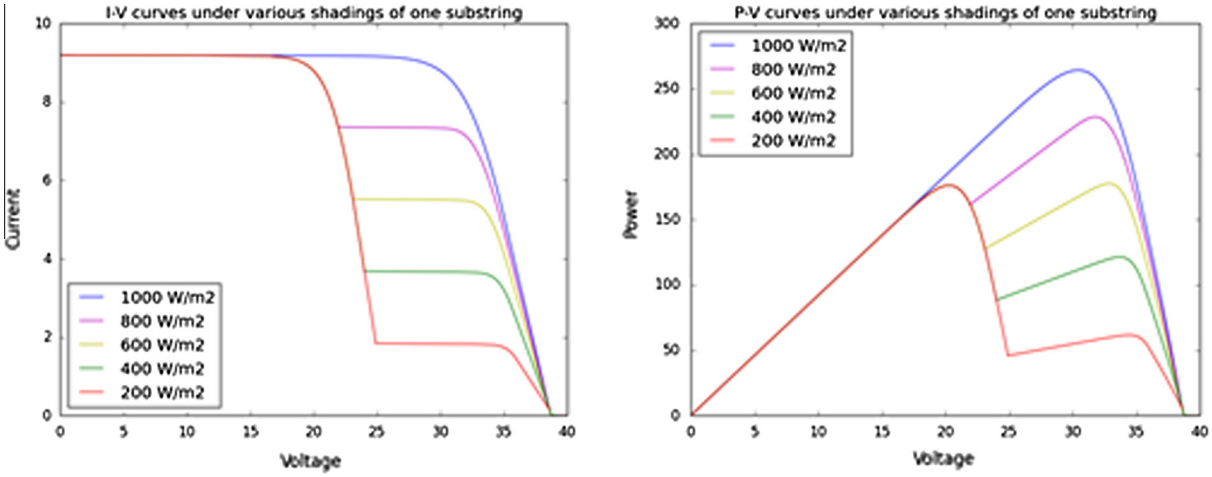

Fig. 3.1.5. Simulated *I–V* and *P–V* curves for the solar module for inhomogeneous irradiance levels.

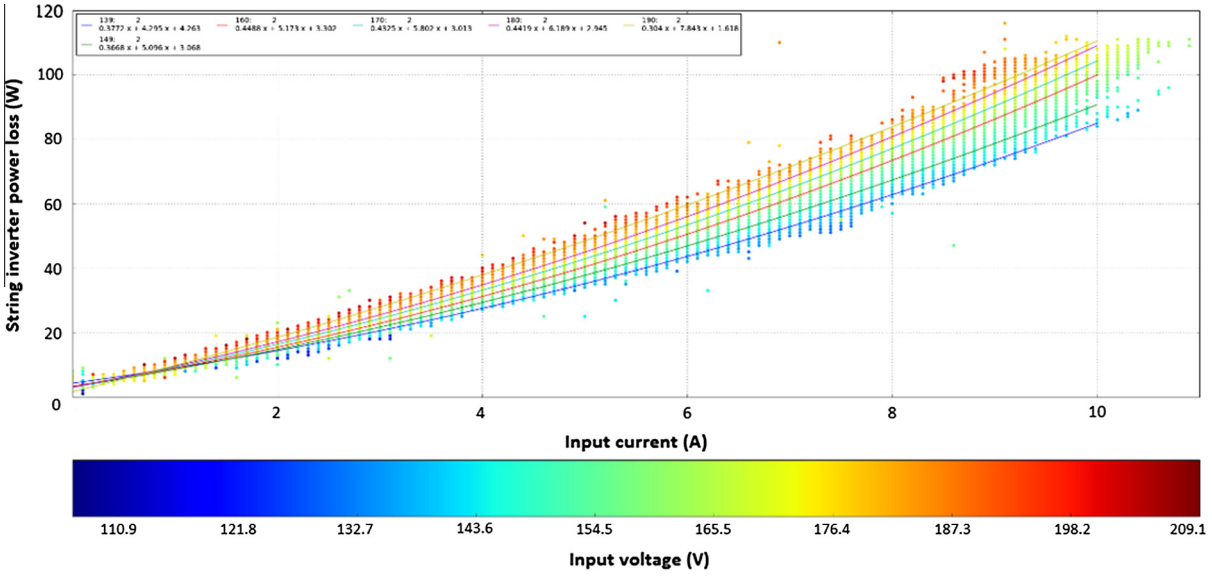

Fig. 3.1.6. Polynomial fit for the power losses of the string inverter for various voltage inputs.

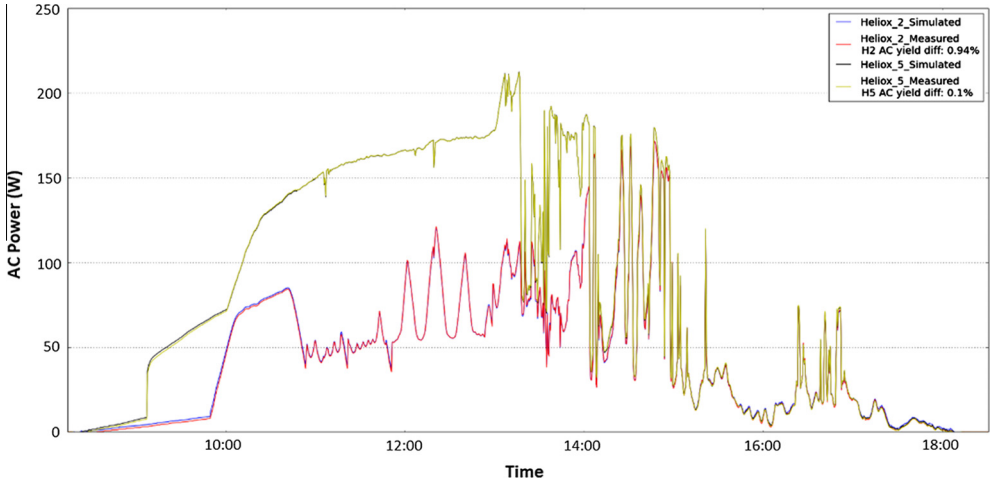

Fig. 3.1.7. Validation of the DC–AC fitting equations for two micro inverters operating with (Heliox 2) and without (Heliox 5) partial shading using real measured and simulated data.

time the algae remains, the more it builds up. In the scenario investigated at this paper the algae covers 2 cm of the bottom of the solar cells.

In Fig. 4.1 the irradiance, the measured and simulated AC power of the three systems can be seen for a clear day without any shading elements. The simulation measurements follow the measured data with high accuracy except early morning and late evening hours when the pyranometer and parts of the PV modules are covered from shade from neighboring buildings. While the system's daily yield is very close for all three systems, the micro inverter (MI) seems to outperform the power optimizer (PO) and string inverter (SI) system by 4.3% and 2.3% respectively. Deviation between measured and simulated daily yield lies below 1% for the power optimizer and micro inverter while it reaches almost 2% for the string inverter system. This occurs partially due to the unavoidable shading late in the evening and because of the increased mismatch losses at high irradiances. When shading is not present hence the mismatch losses are low, the performance of the systems highly depends on the converting efficiency of the power electronics. This issue has been discussed before (Sinapis et al., 2015) and results showed that the converting efficiency of the string inverter especially in low power is superior to the MLPE devices examined in this work.

In Fig. 4.2 partial shading by a pole has been introduced for the three systems. The simulated and measured AC outputs seem to overlap for the most part of the day. The micro inverter and power optimizer systems outperform the string inverter system both in the measured and simulated daily yield data by 7–9%. Small variations occur from the measured data due to the shading fraction detection from the 3D model and the MPP tracker. Specifically for the string inverter system, it is visible how the MPPT is losing the global maximum 3 times during the day and thus reducing the system yield. The detection of this behavior from the simulation model is not possible due to the fact that the tracking algorithm is not known. Measured and simulated daily yield has a deviation of 2.5–3.5% for the MLPE and around 6% for the string inverter system.

In Fig. 4.3 the AC output and irradiance during a clear winter day can be seen. During winter months row to row shading is present due to the wall situated at the south of the systems and because of the distance between the two rows of modules. The systems are gradually free of shade with the power optimizer performing better due to the fact that it can detect the global MPP even at low voltage inputs (up to 8 V). The string inverter system cannot detect the MPP when the voltage input becomes less that 110–120 V and thus operates the PV modules at a local maxima. Therefor the MLPE retrieve 10–11% more energy yield for this specific day. Deviation of simulated and measured data range from 0.5–2.5% for the MLPE and around 4% for the string inverter system.

5. Simulations of monthly and annual yield for various locations and shade scenarios

By using typical meteorological year's irradiation data by Meteonorm (http://meteonorm.com, 2015), a full year simulation for unshaded and partially shaded scenarios has been performed. Meteonorm provides measured irradiance data for a variety of locations. Moreover, the data can be decomposed and transpositioned by using known irradiance models. A constant albedo factor of 0.15 has been used for the simulations. In Fig. 5.1 the monthly simulated losses associated with pole shading can be seen. In this scenario the unshaded yield of the systems serves as reference for the comparison.

During months when shade extension is long due to the low elevation angle of the sun, MLPE systems retrieve significantly more energy, while on summer months where the sun elevation is high the shade impact is much less for all three systems. Monthly energy losses show that there is a strong seasonal variation of yield but on a yearly basis the differences from unshaded to pole shading are around 4% for the MLPE systems and 6.6% for the string inverter system for Eindhoven (Fig. 5.2).

In Fig. 5.2 the AC yield for all shading scenarios and systems can be seen. In the unshaded scenario the string inverter seems to outperform the MLPE systems. This is due to higher operation effi-

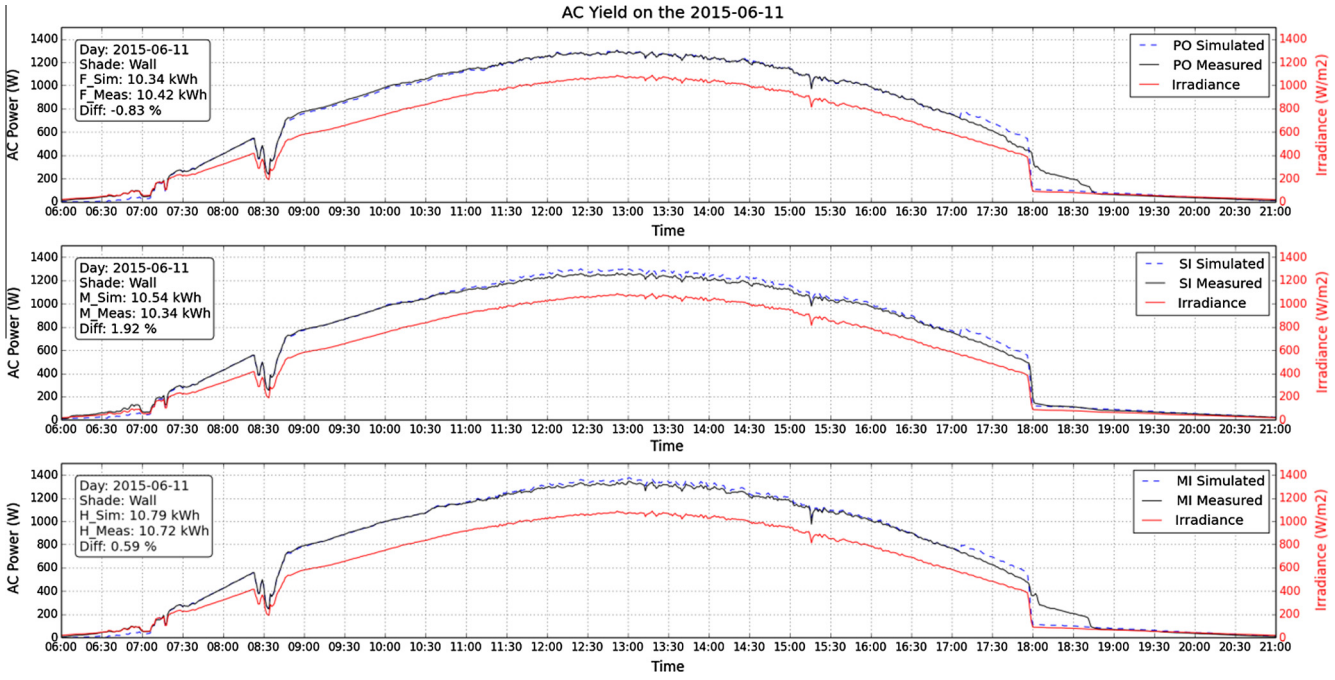

Fig. 4.1. Irradiance, measured and simulated AC output of the three systems for a clear day.

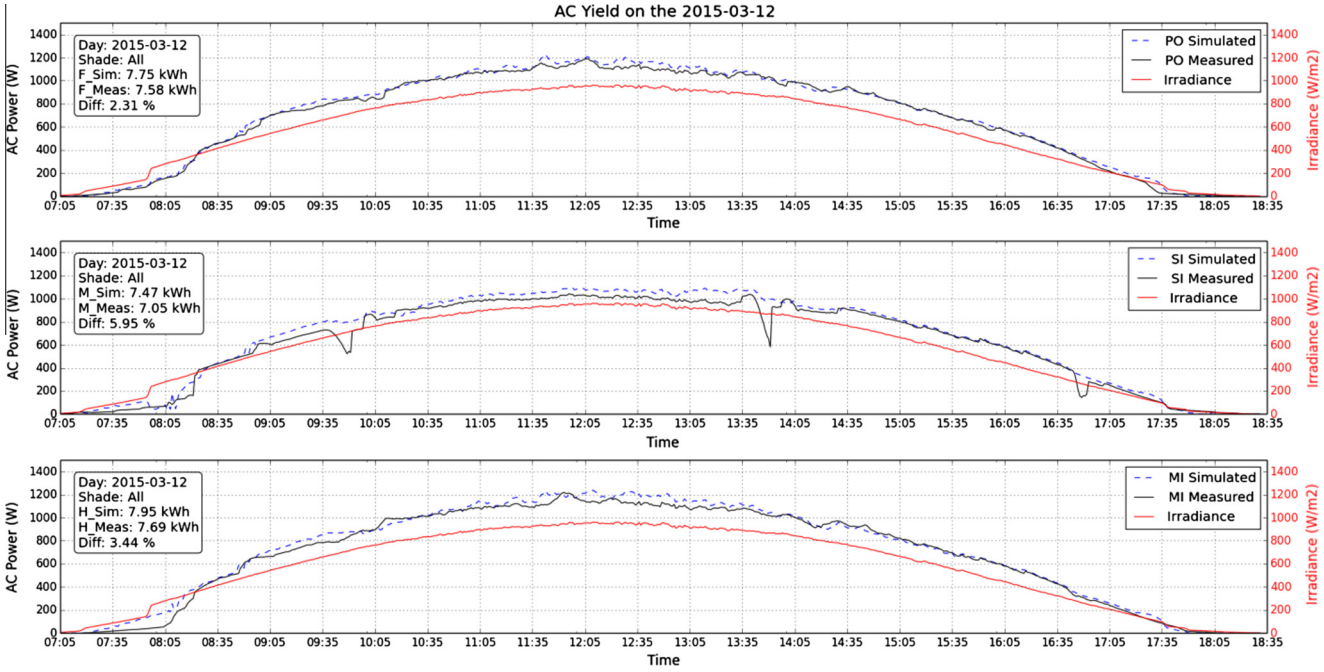

Fig. 4.2. Irradiance, measured and simulated AC power for partial shading by a pole.

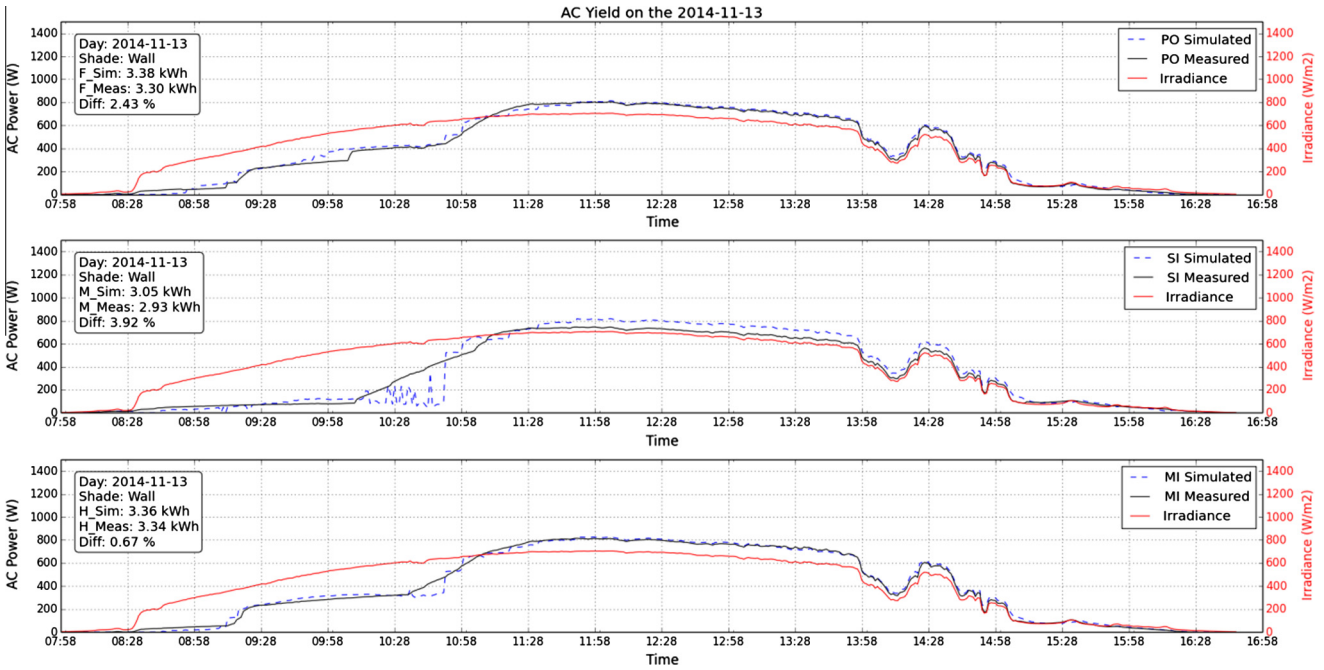

Fig. 4.3. Irradiance, measured and simulated AC power for row to row shading.

ciency of the string inverter system. Surprisingly the string inverter system outperforms MLPE systems at the soiling and row to row shading scenario while the micro inverter system outperforms the rest at the pole shading scenario. While differences of up to 30% on a daily basis have been measured between MLPE and string inverters, on a yearly basis shade impact is modest and especially for central and north European climate which is dominated by low irradiance levels during winter months. However the contribution of summer months in the annual yield has a larger impact than in winter months. As a rule of thumb, system designers and installers evaluate shade extensions and patterns for winter months and avoid installing modules in shade problematic areas. It seems that this approach is very conservative taking into account the results from this study and the current module prices.

Simulations with different irradiation profiles give us further insight on the benefit of MLPE when partial shading is present (Fig. 5.3). Results indicate that the higher the irradiance, the higher the benefit of the micro inverter system. MLPE systems are based on a "pay more get more" philosophy. This means that the increased purchase price of MLPE systems should offer more annual yield and thus accelerate the payback period. Therefor potential investors should evaluate the benefit of MLPE system or string inverter system and determine the financial feasibility of such systems.

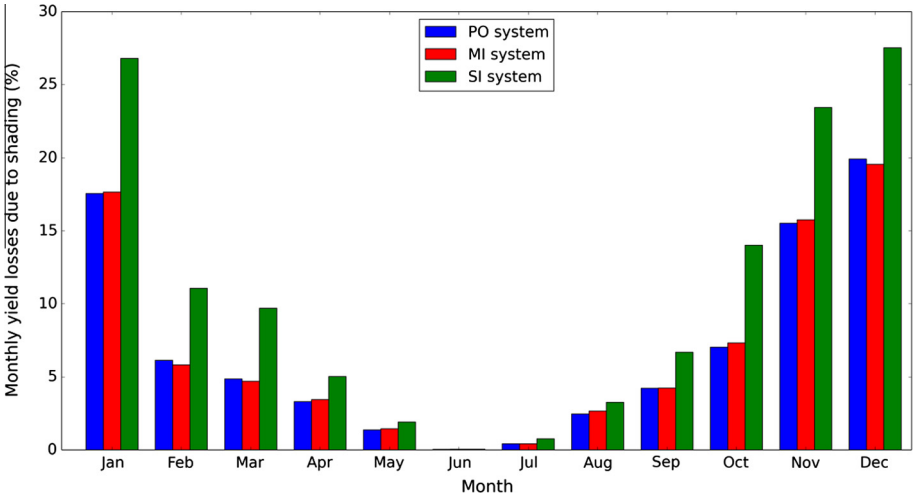

Fig. 5.1. Simulated monthly yield losses for the three systems when shaded by a pole.

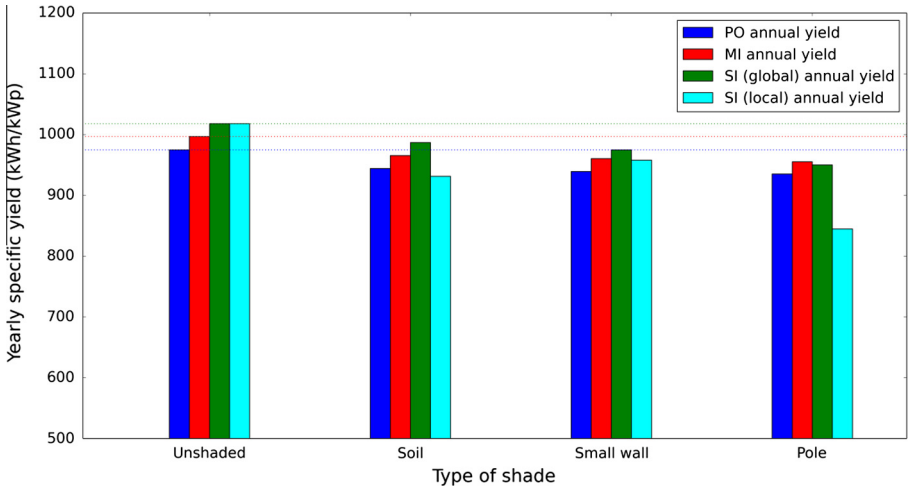

Fig. 5.2. Annual yield simulations for three system architectures under three shading scenarios.

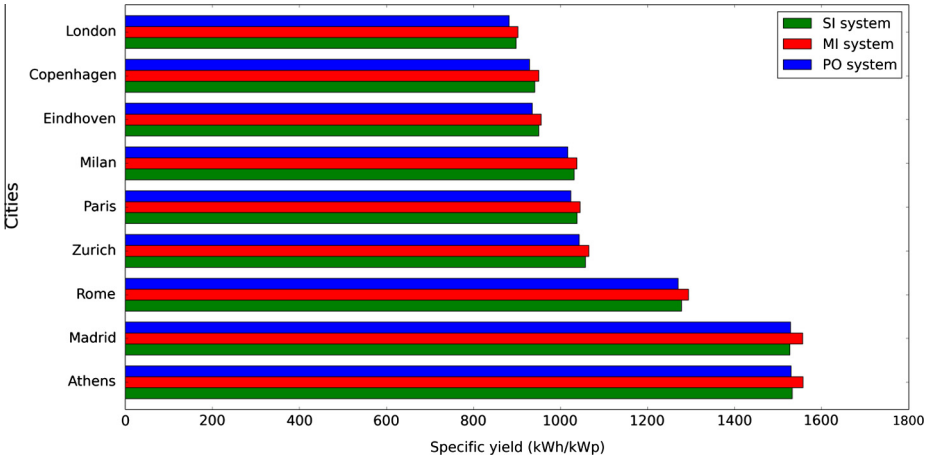

Fig. 5.3. Annual yield simulations for major European cities with different irradiance profiles under partial shading by pole.

6. Conclusions

In this paper an effort was done to assess the shade response of typical c-Si solar modules and different PV system architectures. The shading impact has been proven to be nonlinear for c-Si solar modules. Shading of half a cell has a power impact of 40 times the shade's physical size. Based on these results an effective irradiance equivalent was used to describe operation of solar cells under

partially shaded conditions. Furthermore a model was developed to predict the shading fraction of cells and modules throughout the year and correlate that with yield output. The model was calibrated by using real measured data from three systems installed in Eindhoven.

Results show that shade impact is surprisingly moderate for many shading scenarios. The biggest impact is observed during winter months when shading losses can reach up to 30% for a string inverter system while shading impact is at its minimum during summer months. The pole shading pattern is considered to be the most detrimental for the string inverter limiting the annual yield by 6.6%. Simulations for major European cities with different irradiance profiles show a marginal benefit of the micro inverter system solutions at high irradiance locations.

References

Angus, R.C., Muneer, T., 1993. Sun position for daylight models: precise algorithms for determination. Light. Res. Technol. 25, 81.

Batzelis, E., Georgilakis, P., Papathanasiou, S., 2015. Energy models for photovoltaic systems under partial shading conditions: a comprehensive review. IET Renew. Power Gener. 9 (4), 340–349 http://www.eternalsun.com/products/solar-simulator (accessed 18 September 2015).

Carrero, C., Rodriguez, J., Ramirez, D., Platero, C., 2010. Simple estimation of PV modules loss resistances for low error modelling. Renew. Energy 35, 1103–1108.

Chih-Tang, S., Noyce, R.N., et al., 1957. Carrier generation and recombination in P–N junctions and P–N junction characteristics. Proc. IRE 45 (9), 1228–1243.

Deline, C., 2009. Partially shaded operation of a grid tied PV system. In: Proc. 34th IEEE Photovoltaic Specialists Conference, pp. 1268–1273.

Grunow, P., Lust, S., Sauter, D., Hoffmann, V., Beneking, C., Litzenburger, B., Podlowski, S., 2004. Weak light performance and annual yield of PV modules and systems as a result of the basic parameter set of industrial solar cells. In: Proc. 19 EUPVSEC, Paris, p. 2190.

Gueymard, C., 2009. Direct and indirect uncertainties in the prediction of tilted irradiance for solar engineering applications. Sol. Energy 83 (3), 432–444.

Hanson, A.J., Deline, C., MacAlpine, S.M., Staruth, J.T., Sullivan, C.R., 2014. Partial-shading assessment of photovoltaic installations via module-level monitoring. IEEE J. Photovolt. 4 (6).

http://files.sma.de/dl/3491/TECHOPTITRAC-AEN082412.pdf (accessed 18 September 2015).

http://meteonorm.com/ (accessed 18 September 2015).

http://www.mastervoltsolar.com/high-yield/ (accessed 18 September 2015).

http://www.sketchup.com/ (accessed 18 September 2015).

IEA PVPS Annual Report, 2014. <http://iea-pvps.org/index.php?id=6&eID=dam_frontend_push&docID=2040> (accessed 16 January 2015).

Ishaque, K., Salam, Z., Syafaruddin, 2011. A comprehensive MATLAB Simulink PV system simulator with partial shading capability based on two-diode model. Sol. Energy 85 (9), 2217–2227.

Jinhui, X., Zhongdong, Y., Bingbing, W., Jun, P., 2009. Design of PV array model based on MTDC/PSCAD. In: Power and Energy Engineering Conference.

Loutzenhiser, P.G., Manz, H., Felsmann, C., Strachan, P.A., Frank, T., Maxwell, G.M., 2007. Empirical validation of models to compute solar irradiance on inclined surfaces for building energy simulation. Sol. Energy 81 (2), 254–267.

Poshtkouhi, S., Palaniappan, V., Fard, M., Trescases, O., 2012. A general approach for quantifying the benefit of distributed power electronics for fine grained MPPT in photovoltaic applications using 3-D modelling. IEEE Trans. Power Electron. 27 (11), 4656–4666.

Reindl, D., Beckman, W., Duffie, J., 1990. Diffuse fraction correlations. Sol. Energy 45 (1), 1–7.

Silvestre, S., Boronat, A., Chouder, A., 2009. Study of by-pass diodes configurations on PV modules. Appl. Energy 86 (9), 1632–1640.

Sinapis, K., Litjens, G., van den Donker, M., Folkerts, W., van Sark, W., 2015. Outdoor characterization and comparison of string and module level power electronics under clear and partially shaded conditions. Energy Sci. Eng. 3, 510–519. http://dx.doi.org/10.1002/ese3.97.

Woyte, A., Nijs, J., Belmans, R., 2003. Partial shadowing of photovoltaic arrays with different system configurations: literature review and field test results. Sol. Energy 74, 217–233.